

SERIES ANOMALIES OF LOW MULTIPOLES OF WMAP AND PLANCK MISSIONS: WHAT ARE THEY?

*O. V. Verkhodanov**

Special Astrophysical Observatory, Nizhnij Arkhyz, Russia

We consider the main anomalies of cosmic microwave background observed at low multipoles of the WMAP and Planck cosmic missions. The possible origin of these features is discussed. We study difference between WMAP and Planck data which is apparently connected with the local sources emission and/or systematics.

PACS: 07.57.Kp; 95.85.Bh; 98.70.Vc

INTRODUCTION

The last decade of the CMB study was marked by several marvelous discoveries which changed the observational cosmology. The main cosmological parameters were measured with two satellites — WMAP and Planck.

The observations of the cosmic microwave background radiation (CMB) by the Wilkinson Microwave Anisotropy Probe** (WMAP) [1–8] were revolutionary in modern cosmology. The data were recorded in five bands: 23 GHz (the K-band), 33 GHz (the Ka-band), 41 GHz (the Q-band), 61 GHz (the V-band) and 94 GHz (the W-band) with the measurements of intensity and polarization. The results of the analysis of these data were the CMB maps of anisotropy and polarization, the maps of foreground components (synchrotron and free-free emission, dust radiation), their power spectrum were as well deduced. For the harmonics of not very high order ($\ell < 100$), a map of CMB anisotropy distribution is listed, reconstructed from the multifrequency observations of foreground components implementing the Internal Linear Combination (ILC) method [1]. The resolution of the CMB map is $40'$. The angular power spectrum of CMB produced by the WMAP experiment allowed one to measure all the main cosmological parameters at the most precise level of observational cosmology (with accuracy less than 10%) [9]. All the observational and calibrated data are stored in the public archive at the WMAP site.

*E-mail: vo@sao.ru

**<http://lambda.gsfc.nasa.gov>

The second set of maps and corresponding data were obtained in the European Space Agency experiment Planck* [10] and produced new possibilities in investigation of foreground components and radio sources in millimeter and sub-millimeter wavelengths. Planck observations were carried out at low frequency instrument (LFI bandwidths: 30, 44, 70 GHz) and high frequency instrument (HFI bandwidths: 100, 143, 217, 353, 545, 857 GHz). The satellite Planck rotated around L2-point in the system Sun–Earth as well as the WMAP earlier. The resolution of the CMB maps is $\sim 5'$. Despite the fact that Planck mission is the secondary for WMAP, it has the better observational parameters: the higher resolution (3 times) allowing one to measure the angular power spectrum to higher harmonics, the higher sensitivity (10 times), and the 9 observational bands improving the procedure of microwave signal component separation. These parameters allowed one to obtain new and independent observational data. The Planck Legacy Archive (PLA*) contains maps of background and foreground components and permits one to investigate the CMB signal at different resolution and to check the CMB anomalous properties detected in the WMAP data [11].

Among the most discussed anomalies violating our expectation from the CMB Gaussian distribution, there are Axis of Evil [12], Cold Spot [13], violation of parity in the power spectrum [14], asymmetry “North–South” in galactic coordinate system [15]. And the Planck data added a new unexpected phenomenon — too low amplitude of low harmonics [16]. All these anomalies occur at the largest angular scales ($\theta > 1^\circ$) and demonstrate observation statistical anisotropy being a sign of non-Gaussianity at low multipoles.

When we consider the origin of any anomaly in the CMB map, we should remember the technological chain (or pipeline) of the process of the CMB data reduction and measurement cosmological parameters. It includes several steps:

- 1) registration of time ordered data (TOD);
- 2) pixelization of CMB data and preparation of multifrequency sky maps;
- 3) component separation and cosmological signal rectification using observational data at different wavelengths;
- 4) statistical analysis of CMB maps;
- 5) harmonic transformations “map–spherical harmonics”;
- 6) calculation and analysis of the angular power spectra $C(\ell)$;
- 7) estimation of cosmological parameters.

There are two basic approaches in understanding of the origin of anomalies. The first one is based on suggestions of complex processes during early stages of the Universe. The second one follows the idea of connection of anomalies with foregrounds and/or data analysis procedures. To distinguish the contribution of

*<http://www.rssd.esa.int/Planck/>

*http://www.sciops.esa.int/index.php?project=planck&page=Planck_Legacy_Archive

different effects, we should look attentively at the observations and data analysis of the CMB.

Two basic properties of CMB allow one to separate its signal from foregrounds: (1) black body emission, so it has the same temperature at all wavelengths and (2) correlation of CMB and foregrounds should be close to zero, because CMB is a random Gaussian process. In the simple case, where the instrumental noise can be neglected and the background components have the same spectrum in the region investigated and differ from each other in different parts of this region only in temperature, the sought ILC temperature can be written as a linear combination of signals from the maps for different frequencies ν_i :

$$T_{\text{ILC}}(p) = \sum_i \zeta_i T_i(p) = \sum_i \zeta_i [T_c(p) + S_i T_f(p)] = T_c(p) + \Gamma T_f(p). \quad (1)$$

Here, $T_i(p) \equiv T(\nu_i, p)$ is the map of the signal observed at the frequency ν_i ; p is the certain pixel of the image; the map of the signal $T_i(p) = T_c(p) + S_i T_f(p)$ is represented as a sum of the CMB maps $T_c(p)$ and the background radiation, and $T_f(p)$ is the distribution of the background radiation temperature. The coefficients ζ_i that are to be determined satisfy the normalization condition $\sum_i \zeta_i = 1$. The notation $\Gamma \equiv \sum_i \zeta_i S_i$ is introduced in (1). The coefficients ζ_i are determined by minimization of the dispersion of $T_{\text{ILC}}(p)$. For this dispersion, we have [4]

$$\sigma_{\text{ILC}}^2 = \langle T_{\text{ILC}}^2(p) \rangle - \langle T_{\text{ILC}}(p) \rangle^2 = \langle T_c^2 \rangle - \langle T_c \rangle^2 + 2\Gamma [\langle T_c T_f \rangle - \langle T_c \rangle \langle T_f \rangle] + \Gamma^2 [\langle T_f^2 \rangle - \langle T_f \rangle^2] = \sigma_c^2 + 2\Gamma \sigma_{cf} + \Gamma^2 \sigma_f^2. \quad (2)$$

Here the angular brackets “ $\langle \dots \rangle$ ” denote averaging over the pixel of the selected region. The minimization of σ_{ILC}^2 ,

$$0 = \frac{\delta \sigma_{\text{ILC}}^2}{\delta \zeta_i} = 2 \frac{\delta \Gamma}{\delta \zeta_i} \sigma_{cf} + 2\Gamma \frac{\delta \Gamma}{\delta \zeta_i} \sigma_f, \quad (3)$$

yields $\Gamma = -\sigma_{cf}/\sigma_f^2$ and

$$T_{\text{ILC}}(p) = T_c(p) - \frac{\sigma_{cf}}{\sigma_f^2} T_f(p).$$

In ideal case, where no correlation between the CMB and the background exists, i.e., $\sigma_{cf} = 0$, the ILC map coincides with the CMB map. Actually, as emphasized in [4], the ILC map is biased toward a decrease in the correlation between the CMB signal and the signal from background components. We note that the different version of the ILC method and its variation exist both in pixel space and in harmonic space [17]. And all the methods use the two main

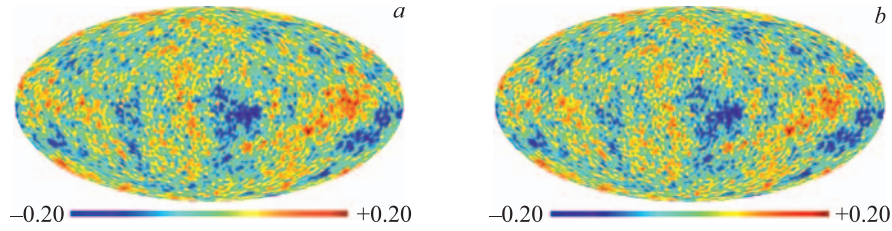


Fig. 1. CMB maps restored from the WMAP (*a*, ILC map) and Planck (*b*, SMICA map) observational data and smoothed up to $\ell_{\max} = 100$

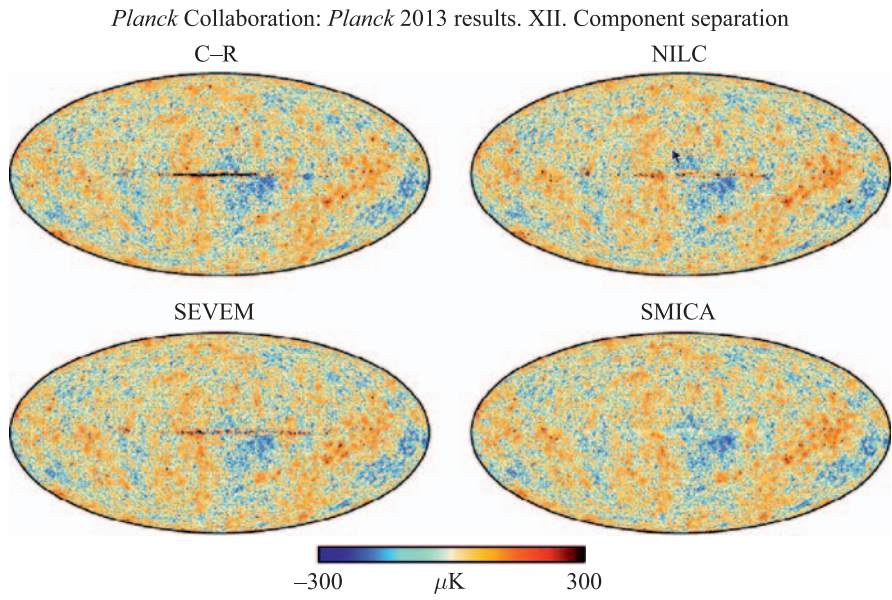


Fig. 2. Four CMB maps (Commander–Ruler, NILC, SEVEM, SMICA) restored by different methods from the Planck observational data

properties mentioned in this paragraph. The maps restored in WMAP and Planck experiments are shown in Figs. 1 and 2.

For the restored CMB signal, the angular power spectrum is calculated using the so-called $a_{\ell m}$ -coefficients:

$$C(\ell) = \frac{1}{2\ell + 1} \left[|a_{\ell 0}|^2 + 2 \sum_{m=1}^{\ell} |a_{\ell m}|^2 \right]. \quad (4)$$

The $a_{\ell m}$ -coefficients are obtained in the standard decomposition of the measured temperature variations on the sky, $\Delta T(\theta, \phi)$, in spherical harmonics (multipoles):

$$\Delta T(\theta, \phi) = \sum_{\ell=2}^{\infty} \sum_{m=-\ell}^{m=\ell} a_{\ell m} Y_{\ell m}(\theta, \phi), \quad (5)$$

$$Y_{\ell m}(\theta, \phi) = \sqrt{\frac{(2\ell+1)(\ell-m)!}{4\pi(\ell+m)!}} P_{\ell}^m(x) e^{im\phi}, \quad x = \cos \theta,$$

where $P_{\ell}^m(x)$ are the associated Legendre polynomials. For a continuous $\Delta T(x, \phi)$ function, the coefficients of decomposition, $a_{\ell m}$, are

$$a_{\ell m} = \int_{-1}^1 dx \int_0^{2\pi} d\phi \Delta T(x, \phi) Y_{\ell m}^*(x, \phi), \quad (6)$$

where $Y_{\ell m}^*$ denotes complex conjugation of $Y_{\ell m}$. This angular spectrum, being the measured characteristics of the CMB, on the one hand, is the function of the main cosmological parameters

$$C_{\ell} \equiv C_{\ell}(h, \Omega_b h^2, \Omega_{CDM} h^2, \Omega_{\Lambda}, \Omega_{\nu}, n, \dots),$$

on the other hand.

1. REVIEW OF THE MAIN ANOMALIES

Below we describe the main anomalies registered in both WMAP and Planck data.

1.1. Axis of Evil. The Axis of Evil (Fig. 3) is the most famous among non-Gaussian features of the WMAP CMB data. The Axis unifies some problems which require special explanations. They are the planarity and alignment of the two harmonics, quadrupole and octupole, and, partly, the problem of extremely low amplitude of the quadrupole. Different estimations of the significance of

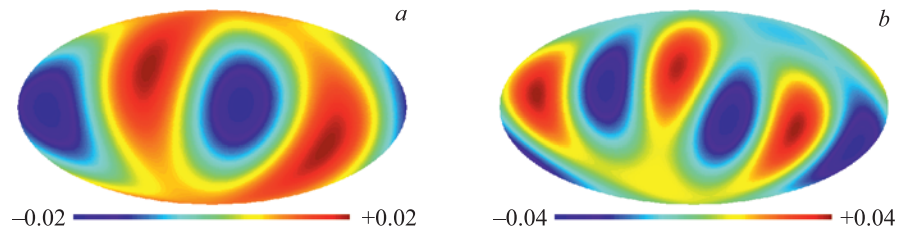


Fig. 3. Axis of Evil: planarity and alignment of the quadrupole (a) and the octupole (b) on the WMAP CMB map

existence of this axis and several hypotheses on its origin were made. Various studies, e.g., [18, 19], investigated the contribution of background components and their influence on the alignment of multipoles ($\ell = 2$ and $\ell = 3$), and indicated a small probability of the background effect on the orientation of the low multipoles. In [18], where the multipole vectors were used for the estimates of this effect, it was also noted that the positions of the quadrupole and octupole axes correspond to the geometry and direction of motion of the Solar System and are perpendicular to the ecliptic plane and the plane given by the direction to the dipole. Randomness of such an effect is estimated by the authors as unlikely at the significance level exceeding 98% and excludes the effect of residual contribution of background components. Continuing the research done, Copi et al. [20] conclude that the characteristics of low multipoles are abnormally different from random, which may be due to the statistical anisotropy of the Universe at large scales, or to the problems of the ILC signal deconvolution method. Park et al. [21] note that the planarity of the quadrupole and octupole is not statistically significant. They also stress that the residual photon radiation in the ILC map does not affect significantly the level of the effect.

Cosmological models were developed to explain the prominence of the axis in the orientation of multipoles. The alignment of the quadrupole and octupole could be explained within the framework of these models. Various models include the anisotropic expansion of the Universe, rotation and magnetic field [22–24].

There are some hints demonstrating that the problem of existence of the Axis of Evil can be connected with the instability of CMB reconstruction at low multipoles ($2 \leq \ell \leq 10$) in ILC method [25,26]. Another possible solution of the problem is to construct the separation methods on the homogeneous samples of pixels where it is possible to tune selection of subsample in such a way that the quadrupole amplitude of the restored map grows and phase changes, so no Axis of Evil exists [27].

The Planck team using new data [16] detected that the angle between planes of quadrupole and octupole is equal to $\sim 13^\circ$ (against $\sim 3^\circ$ or $\sim 9^\circ$ for WMAP data in different observational years) and declared that significance of the quadrupole–octupole alignment is substantially smaller than for the WMAP data, falling to almost 98% confidence level for the Commander–Ruler and SEVEM maps and 96.7% confidence level for the NILC map. However, later, Copi et al. [28] demonstrated that the WMAP and Planck data confirm the alignments of the largest observable CMB modes in the Universe. Using different statistical methods to control the mutual alignment between the quadrupole and octupole, and the alignment of the plane defined by the two harmonics with the dipole direction, the authors obtained that both phenomena are at the greater than 3σ level for three Planck maps (SMICA, SEVEM, NILC) studied.

1.2. Cold Spot. The next excited feature discussed in Introduction is the Cold Spot (CS) (Fig. 4). This is a cold region exhibiting a complex structure identified

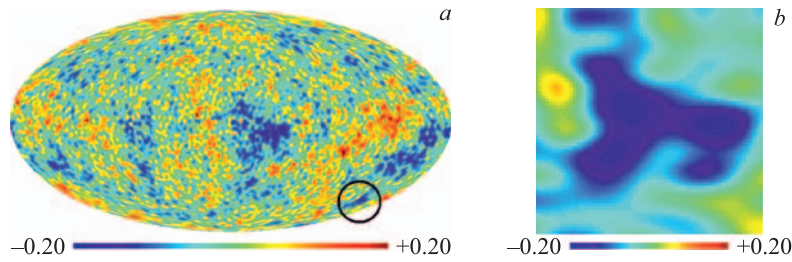


Fig. 4. Cold Spot: position of the Cold Spot on the WMAP CMB map (*a*) and its shape (*b*)

in the CMB using spherical Mexican hat wavelets [13]. The non-Gaussianity of the signal in the Southern hemisphere was explained precisely by the existence of this region. The galactic coordinates of center of the spot are $b = -57^\circ$, $l = 209^\circ$. The probability of the signal in CS being consistent with the Gaussian model if spherical wavelets are used is about 0.2% [13]. After obtaining indication of the signal non-Gaussianity at the CS as well as messages on the reduced density of source [29] in smoothed maps of radio survey NVSS at 1.4 GHz [30], several hypotheses concerning the origin of the Cold Spot were discussed which were related to the intergated Sachs–Wolfe effect [29], the topological defect [31], anisotropic expansion [32], the artefact of data analysis [33], and simply a random deviation [11].

As was noted in [33], the possible galactic foreground residuals in the CMB maps can produce such a type of the spot as a part of non-Gaussianity at low multipoles. We should add that the CS is also manifested in the data of 1982 in maps of a low-frequency survey [34] where synchrotron radiation contributes significantly to the background (Fig.5). In favor of the hypothesis of the CS being the Galactic phenomena, the following fact testifies. There exists a high

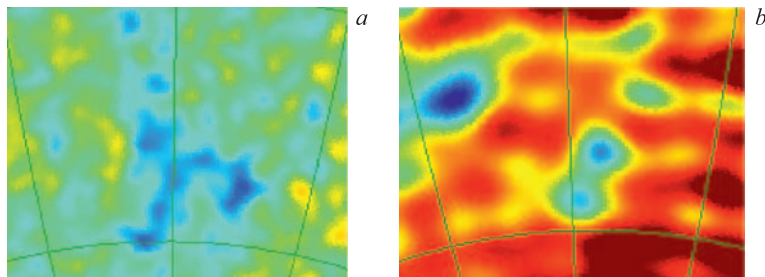


Fig. 5. Cold Spot on the WMAP CMB map (*a*) and 408 MHz map (*b*) with synchrotron emission

correlation of positions of peaks of CMB fluctuataion and galactic magnetic field distribution [35].

1.3. Violation of the Power Spectrum Parity. A remarkable manifestation of non-Gaussian properties of low multipoles consists in parity asymmetry first noticed in [14] and confirmed in Planck data [16]. For a Gaussian random field of primary perturbations $\Phi(k)$ with a flat power spectrum, the presence of a plateau in the CMB angular power spectrum is expected at low multipoles, which is due to the Sachs–Wolfe effect, namely, to the fact that $\ell(\ell + 1)C_\ell \approx \text{const}$. Spherical harmonics change as $Y_{\ell m}(\hat{\mathbf{n}}) = (-1)^\ell Y_{\ell m}(-\hat{\mathbf{n}})$ when the coordinates are reversed. Therefore, an asymmetry in the angular power spectrum for even and odd harmonics can be regarded as the asymmetry of the power of even and odd components of map. The authors [14] found the power of odd multipoles to systematically exceed the power of even multipoles of low ℓ and termed this phenomenon “parity asymmetry”. To describe such an asymmetry qualitatively, the following quantities are proposed for consideration:

$$P^+ = \sum_{\text{Even } \ell < \ell_{\max}} \ell(\ell + 1)C_\ell / 2\pi,$$

$$P^- = \sum_{\text{Odd } \ell < \ell_{\max}} \ell(\ell + 1)C_\ell / 2\pi.$$

Using the data of WMAP power spectrum and the results of Monte Carlo simulations, the authors [14] calculated the ratio P^+/P^- for the multipole ranges $2 \leq \ell \leq \ell_{\max}$, where ℓ_{\max} lies between 3 and 23. Comparing P^+/P^- for the WMAP data with a similar ratio obtained for simulated maps allows estimating the quantity p equal to the fraction of simulated spectra in which P^+/P^- is less than or equal to the same quantity for the WMAP map. The value of p was found to reach its lower boundary at $\ell_{\max} = 18$, where p equals 0.004 and 0.001 for the data obtained by the WMAP mission during five and three years of observations, respectively. This fact means that there is a preference for odd multipoles $2 \leq \ell \leq 18$ in the WMAP data at a confidence level of 99.6% with a screening mask imposed on the data, and of 99.76% without any mask. The authors believe the low amplitude of the WMAP CMB quadrupole may be part of the same anomaly as the parity asymmetry. Because the power asymmetry of the CMB signal in the Northern and Southern hemispheres is manifested more strongly in the case of multipoles with $2 \leq \ell \leq 19$ than multipoles with $20 \leq \ell \leq 40$, the authors also believe that the general origin of anomalies (such as the power asymmetry in the hemispheres, the low quadrupole amplitude, and the parity asymmetry) lies in the region of small ℓ and that the explanation can be either cosmological or related to the presence of systematic errors in observations that were not revealed and/or were additionally introduced in the course of analysis of the data obtained by the WMAP mission.

1.4. Hemispherical Asymmetry. The asymmetry of hemispheres (see, e.g., Fig. 1) was detected just after publishing the first year all sky maps of the WMAP [15]. Then, in [36], some calculations based on the angular power spectrum were presented and it was shown that this spectrum, when estimated locally at different positions on the sphere, appears not to be isotropic. Park [37] also presented evidence for the existence of such a hemispherical asymmetry, in which a particular statistical measure is considered to change discontinuously between two hemispheres on the sky, applying Minkowski functionals to the WMAP data. Since the preferred direction, according to Eriksen et al. [15], lies close to the ecliptic plane, it was also demonstrated that the large-angular scale N-point correlation functions were different in behavior when computed on ecliptic hemispheres.

Several studies were focused on the hemisphere difference and its connection with the ecliptic coordinate system [38–40]. Hemispherical asymmetry was also detected with other measures of non-Gaussianity [41–43]. The Planck team repeated the analysis [42] on the Planck component separated data. As was shown in [16], the probabilities of obtaining a value for the χ^2 Planck fiducial Λ CDM model are different both for North and for South. For example, using SMICA map, one obtains 0.932 for Northern ecliptic and 0.592 for Southern ecliptic hemispheres. Thus, the observed properties of the Planck data are consistent with a remarkable lack of power in a direction towards the north ecliptic pole, consistent with the simpler one-point statistics [16].

2. DIFFERENCE OF THE WMAP AND PLANCK ANGULAR POWER SPECTRA

One of the main anomalies first detected in the Planck data was the lack of power at low multipoles detected for angular power spectrum $C(\ell)$ (Fig. 6). Using the WMAP and Planck officially published spectra, we can compare them via the calculation of the difference of maps including only the harmonics with maximum $C(\ell)$ difference (Fig. 7).

Following [44], let us consider the differences of maps corresponding to the harmonics having the maximum difference of power. These ranges are marked by rectangles in Fig. 7. The vertical lines demonstrate limits of the multipole range in $\ell \in [41; 46]$. In Figs. 8–10 are shown maps of harmonic differences at $\ell = 3$, $\ell = 5$, $\ell = 7$, respectively. Some features of these differences show the position of spots along the Galactic plane, sensitivity of difference map at $\ell = 5$ to the equatorial coordinate system (equatorial poles are placed in singular points — saddles), and the axis of the multipole $\ell = 7$ lies on the Galactic plane and, simultaneously, the saddle points of $\ell = 7$ are placed in ecliptic poles.

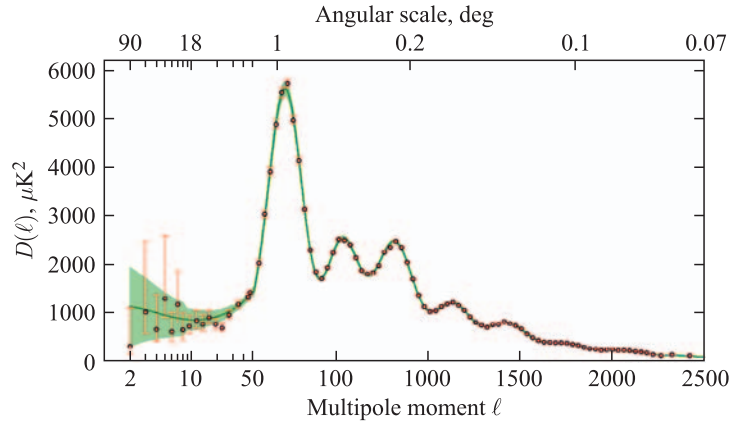


Fig. 6. CMB angular power spectrum of the 1st Planck data release

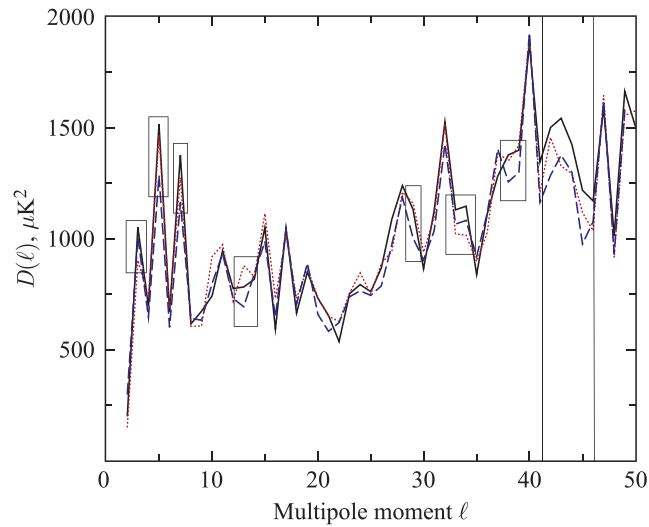


Fig. 7. The angular power spectrum $D(\ell) = \ell(\ell + 1)C_\ell/2\pi$ in the multipole $2 \leq \ell < 50$. The solid line shows WMAP ILC data of the 7th year of observations. The dotted line marks WMAP9 ILC data, the Planck data are marked by the dashed line. The rectangles show the most different angular moments of distributions. The vertical lines mark limits of the multipole range in $\ell \in [41; 46]$

At the scales less 20° , there are three harmonics $\ell = 13$ (Fig. 11), $\ell = 29$ (Fig. 12), $\ell = 37$ (Fig. 13) which have the maximum difference in power. Following the difference of signal at the selected multipole maps, we can find the features close to the ones detected earlier.

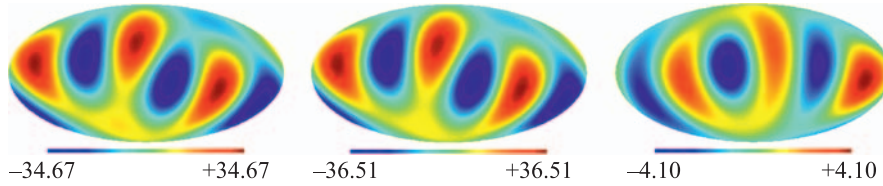


Fig. 8. Left to right: the octupole ($\ell = 3$) of the Planck CMB map SMICA, the octupole of the ILC WMAP9 map, and the map of these signals difference

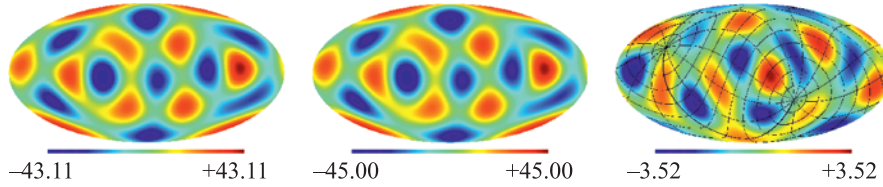


Fig. 9. Left to right: the map of $\ell = 5$ of the Planck CMB map SMICA, the $\ell = 5$ of the ILC WMAP9 map, and the map of these signals difference. The equatorial coordinate grid is overlaid on the map of difference

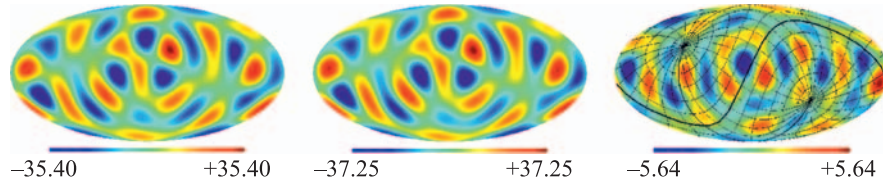


Fig. 10. Left to right: the map of $\ell = 7$ of the Planck CMB map SMICA, the $\ell = 7$ of the ILC WMAP9 map, and the map of these signals difference. The ecliptic coordinate grid is overlaid on the map of difference

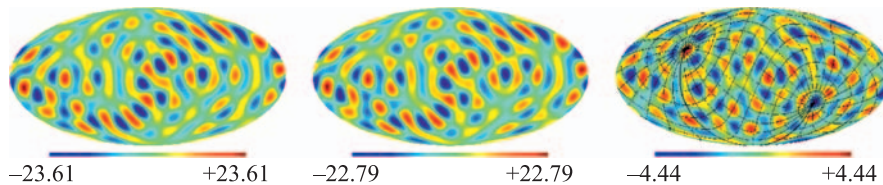


Fig. 11. Left to right: the map of $\ell = 13$ of the Planck CMB map SMICA, the $\ell = 13$ of the ILC WMAP9 map, and the map of these signals difference. The ecliptic coordinate grid is overlaid on the map of difference

The map of multipole difference at $\ell = 13$ (angular size of $\sim 6.5^\circ$) contains a feature similar to the harmonic $\ell = 7$, where the ecliptic poles are placed in singular points — local map minima and maxima. The multipole difference at

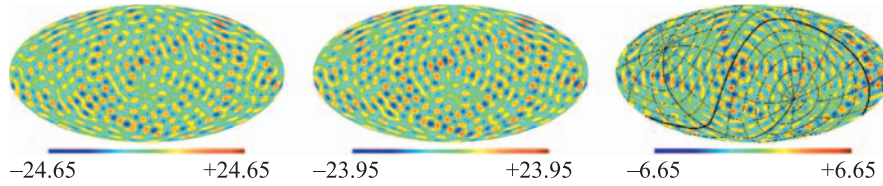


Fig. 12. Left to right: the map of $\ell = 29$ of the Planck CMB map SMICA, the $\ell = 29$ of the ILC WMAP9 map, and the map of these signals difference. The equatorial coordinate grid is overlaid on the map of difference

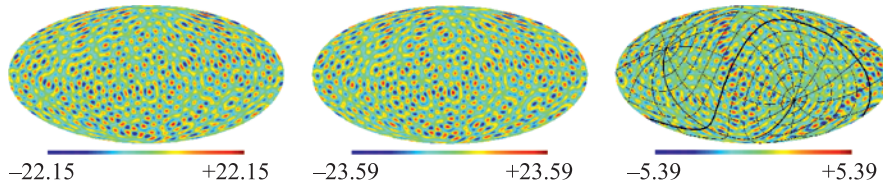


Fig. 13. Left to right: the map of $\ell = 37$ of the Planck CMB map SMICA, the $\ell = 37$ of the ILC WMAP9 map, and the map of these signals difference. The equatorial coordinate grid is overlaid on the map of difference

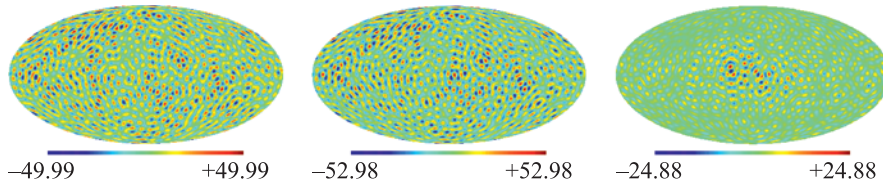


Fig. 14. Left to right: the summarized signal of multipole $\ell \in [41; 46]$ for the Planck CMB map SMICA, harmonics $\ell = 41-46$ of WMAP9 ILC, and map of difference of these signals

the scales $\ell = 29$ ($\sim 3^\circ$) and $\ell = 37$ ($\sim 2.5^\circ$) contains a similar structure of spots placement. One line drawn by the very contrast spots formed with m -modes combinations of the $\ell = 29$ and $\ell = 37$ coincides with the ecliptic plane. Curiously, a structure of the bright spots placement for $\ell = 29$ and $\ell = 37$ in the right hemisphere corresponds to the anisotropic model Bianchi_{VIII} discussed in [16]. There is a range of multipoles ($\ell \in [41; 46]$) where the spectrum strongly differs for the WMAP and Planck data (Figs. 7 and 14). The map difference for these multipoles range shows the extended structure near the Galactic center.

Note that there are two important moments observed in multipole differences. First, all the maps of multipole difference with high amplitude contain features tied with galactic, ecliptic or/and equatorial (terrestrial) coordinate systems. Second,

there is a $\Delta\ell = 8$ period for multipoles numbers having a big difference in amplitude. Peculiar harmonics have numbers $\ell = 5, 13, 29, 37, 45$.

SUMMARY

As we can see from the details of the CMB anomalies mentioned above, most of them manifest the properties sensitive to local environment. Three main environments of the cosmic observatory are displayed in the CMB signal distribution. They are our Galaxy — Milky Way, the Solar (ecliptic) system and some features connected with the equatorial system. The Galaxy is a source of the non-Gaussian residuals visible in positions of CMB spots (see discussion in [45]). The Cold Spot is a special feature visible in synchrotron emission and on a map of the distribution of the Faraday rotation depth. Thus, it is probably connected with an ionized cloud from Galaxy or its vicinity.

The Solar system objects are considered as a source of additional residuals on the CMB map which are difficult to account in the standard component separation methods. Possible sources of residual signal are the satellite antenna far sidelobes sensitive to the Sun and bright planets, solar wind focusing by the Earth magnetosphere and passing through the Lagrange point L2, the objects at boundary of Solar system like the Kuiper belt.

The equatorial system features detected in some CMB correlation maps or in the single harmonic maps can be due to the influence of the Earth microwave emission also through the antenna back lobes or possible Solar wind emission modulated by the Earth magnetosphere where the magnetic axis is close to the Earth rotation axis.

All these explanations may shed light to origin of CMB low multipoles anomalies. The mismatch of the WMAP and Planck data, on the one hand, and BICEP2 [46] results of B-mode polarization, on the other hand, connected with an amplitude of angular power spectrum can also be considered as a problem of low multipoles. For example, the authors of [47] demonstrated that effect of the charged dust emission connected with the Galaxy synchrotron loops can manifest some anomalies at low polarization harmonics and, thus, should be taken into account when microwave components of a signal are separated.

Also it is necessary to note that there are some anomalies in the Planck data detected at high ($\ell > 600$) harmonics. There is a disagreement between cosmological parameters determination using the CMB angular power spectrum (including or not other experiments) and using only the Sunyaev–Zeldovich clusters [48]. Such a disaccord, as discussed also in this paper, can be explained by the biased estimates cluster parameters with the X-ray data.

Another reason of anomalies is some kinds of systematics in data analysis. There is a comparatively small difference (about 1.1σ) between cosmological

parameters determined with the WMAP and Planck data [49]. The authors of paper [50] discussed this difference and repeated the component separation procedure using Planck multifrequency observational maps. They detected that in case of excluding the Planck 217 GHz channel from the data processing, the cosmological parameters measured with the WMAP9 data are restored by the Planck observations with the high accuracy ($< 1.1\sigma$). The authors of [50] conclude that there exists some problem in the calibration of this channel data.

Thus, we can say that:

1. WMAP and Planck data have practically the same low multipole anomalies;
2. All the visible anomalies can be understood in the framework of the local (galactic and ecliptic) sources of microwave emission;
3. The difference of WMAP and Planck power spectra looks like one due to systematic effects of maps preparation;
4. Planck data are comparatively good (in resolution and sensitivity) when we take into account strangeness, e.g., some “bad” multipoles and 217 GHz data;
5. We are waiting for a new release in the second half of 2014: maps of temperature anisotropy and polarization.

And finishing this review and following the topic of the Workshop, I give some neutrino parameters determined with the Planck data from the paper [49] for extended concordance Λ CDM cosmological model and considered as separate cases:

1)

$$\sum m_\nu < \begin{cases} 0.98 \text{ eV} & (95\%; \text{Planck} + \text{WMAP pol.} + \text{Planck high } \ell), \\ 0.32 \text{ eV} & (95\%; \text{Planck} + \text{WMAP pol.} + \text{Planck high } \ell + \text{BAO}); \end{cases}$$

2)

$$N_{\text{eff}} = 3.52^{+0.48}_{-0.45} \quad (95\%; \text{Planck} + \text{WMAP pol.} + \text{Planck high } \ell + H_0 + \text{BAO});$$

3)

$$\left. \begin{array}{l} N_{\text{eff}} = 3.32^{+0.54}_{-0.52} \\ \sum m_\nu < 0.28 \text{ eV} \end{array} \right\} (95\%; \text{Planck} + \text{WMAP pol.} + \text{Planck high } \ell + \text{BAO});$$

4)

$$\left. \begin{array}{l} N_{\text{eff}} < 3.80 \\ m_{\nu, \text{sterile}}^{\text{eff}} < 0.42 \text{ eV} \end{array} \right\} (95\%; \text{Planck} + \text{WMAP pol.} + \text{BAO for } m_{\text{sterile}}^{\text{therm}} < 10 \text{ eV}).$$

Acknowledgements. The author is thankful to the Organizing Committee for hospitality and invitation to the Workshop. The author is also grateful to NASA for possibility to use NASA Legacy Archive where WMAP maps are stored and

ESA for open access to observational results in Planck Legacy Archive. The GLESP* package [51] was used to process the CMB maps on a sphere. The explorations in this topic were supported by the RFBR, grant No. 13-02-00027.

REFERENCES

1. *Bennett C.L. et al. (WMAP Collab.).* First-Year Wilkinson Microwave Anisotropy Probe (WMAP) Observations: Preliminary Maps and Basic Results // *Astrophys. J. Suppl.* 2003. V. 148. P. 1; arXiv:astro-ph/0302207.
2. *Bennett C.L. et al. (WMAP Collab.).* First-Year Wilkinson Microwave Anisotropy Probe (WMAP) Observations: Foreground Emission // *Astrophys. J. Suppl.* 2003. V. 148. P. 97; arXiv:astro-ph/0302208.
3. *Spergel D.N. et al. (WMAP Collab.).* First Year Wilkinson Microwave Anisotropy Probe (WMAP) Observations: Determination of Cosmological Parameters // *Astrophys. J. Suppl.* 2003. V. 148. P. 175; arXiv:astro-ph/0302209.
4. *Hinshaw G. et al. (WMAP Collab.).* Three-Year Wilkinson Microwave Anisotropy Probe (WMAP) Observations: Temperature Analysis // *Astrophys. J. Suppl.* 2007. V. 170. P. 288; arXiv:astro-ph/0603451.
5. *Spergel D.N. et al. (WMAP Collab.).* Wilkinson Microwave Anisotropy Probe (WMAP) Three-Year Results: Implications for Cosmology // *Astrophys. J. Suppl.* 2007. V. 170. P. 377; arXiv:astro-ph/0603449.
6. *Hinshaw G. et al. (WMAP Collab.).* Five-Year Wilkinson Microwave Anisotropy Probe (WMAP) Observations: Data Processing, Sky Maps, and Basic Results // *Astrophys. J. Suppl.* 2009. V. 180. P. 225; arXiv:astro-ph/0803.073).
7. *Komatsu E. et al. (WMAP Collab.).* Five-Year Wilkinson Microwave Anisotropy Probe (WMAP) Observations: Cosmological Interpretation // *Astrophys. J. Suppl.* 2009. V. 180. P. 330; arXiv:0803.0547.
8. *Jarosik N. et al. (WMAP Collab.).* Seven-Year Wilkinson Microwave Anisotropy Probe (WMAP) Observations: Sky Maps, Systematic Errors, and Basic Results // *Astrophys. J. Suppl.* 2011. V. 192. P. 14; arXiv:1001.4744.
9. *Bennett C.L. et al.* Nine-Year Wilkinson Microwave Anisotropy Probe (WMAP) Observations: Final Maps and Results // *Astrophys. J. Suppl.* 2013. V. 208. P. 20; arXiv:1212.5225.
10. *Ade P. A. R. et al. (Planck Collab.).* Planck 2013 Results. I. Overview of Products and Scientific Results // *Astron. Astrophys.* 2013 (in press); arXiv:1303.5062.
11. *Bennett C.L. et al. (WMAP Collab.).* Seven-Year Wilkinson Microwave Anisotropy Probe (WMAP) Observations: Are There Cosmic Microwave Background Anomalies? // *Astrophys. J. Suppl.* 2011. V. 192. P. 17; arXiv:1001.4758.

*<http://www.glesp.nbi.dk>

12. *Land K., Magueijo J.* Examination of Evidence for a Preferred Axis in the Cosmic Radiation Anisotropy // *Phys. Rev. Lett.* 2004. V. 95g. P. 1301.
13. *Cruz M. et al.* Detection of a Non-Gaussian Spot in WMAP // *MNRAS.* 2005. V. 356. P. 29.
14. *Kim J., Naselsky P.* Anomalous Parity Asymmetry of the Wilkinson Microwave Anisotropy Probe Power Spectrum Data at Low Multipoles // *Astrophys. J.* 2010. V. 714. P. L265.
15. *Eriksen H.K. et al.* Asymmetries in the Cosmic Microwave Background Anisotropy Field // *Astrophys. J.* 2004. V. 605. P. 14.
16. *Ade P. A. R. et al. (Planck Collab.).* Planck 2013 Results. XXIII. Isotropy and Statistics of the CMB // *Astron. Astrophys.* 2003 (in press); arXiv:1303.5083.
17. *Leach S.M. et al. (Planck Collab.).* Component Separation Methods for the PLANCK Mission // *Astrophys.* 2008. V. 491. P. 597; arXiv:0805.0269.
18. *Copi C.J. et al.* On the Large-Angle Anomalies of the Microwave Sky // *MNRAS.* 2006. V. 367. P. 79; arXiv:astro-ph/0508047.
19. *Gruppuso A., Burigana C.* Large Scale Alignment Anomalies of CMB Anisotropies: A New Test for Residuals Applied to WMAP 5 yr Maps // *JCAP.* 2009. V. 08. P. 004.
20. *Copi C.J. et al.* No Large-Angle Correlations on the Non-Galactic Microwave Sky // *MNRAS.* 2009. V. 399. P. 295.
21. *Park C.-G., Park C., Gott III J.R.* Cleaned 3-Year Wilkinson Microwave Anisotropy Probe Cosmic Microwave Background Map: Magnitude of the Quadrupole and Alignment of Large-Scale Modes // *Astrophys. J.* 2007. V. 660. P. 959; arXiv:astro-ph/0608129.
22. *Jaffe T.R. et al.* Bianchi Type VIII Models and the WMAP 3-Year Data // *Astron. Astrophys.* 2006. V. 460. P. 393.
23. *Demianski M., Doroshkevich A. G.* Extensions of the Standard Cosmological Model: Anisotropy, Rotation, and the Magnetic Field // *Phys. Rev. D.* 2007. V. 75l. P. 3517.
24. *Koivisto T., Mota D.F.* Anisotropic Dark Energy: Dynamics of the Background and Perturbations // *JCAP.* 2008. V. 06. P. 018.
25. *Naselsky P.D., Verkhodanov O. V.* Do We Need to Correct the Internal Linear Combination Quadrupole? // *Astrophys. Bull.* 2007. V. 62. P. 203.
26. *Naselsky P.D., Verkhodanov O. V., Nielsen M. T. B.* Instability of Reconstruction of the Low CMB Multipoles // *Astrophys. Bull.* 2008. V. 63. P. 216; arXiv:0707.1484.
27. *Doroshkevich A. G., Verkhodanov O. V.* CMB Component Separation in the Pixel Domain // *Phys. Rev. D.* 2011. V. 83. P. 3002; arxiv:1008.4094.
28. *Copi C.J. et al.* Large-Scale Alignments from WMAP and Planck. arXiv:1311.4562.
29. *Rudnick L., Brown S., Williams L.R.* Extragalactic Radio Sources and the WMAP Cold Spot // *Astrophys. J.* 2007. V. 671. P. 40; arXiv:0704.0908.
30. *Condon J.J. et al.* The NRAO VLA Sky Survey // *Astronom. J.* 1998. V. 115. P. 1693.

31. *Cruz M. et al.* A Cosmic Microwave Background Feature Consistent with a Cosmic Texture // *Science*. 2007. V. 318. P. 1612; arXiv:0710.5737.
32. *Jaffe T. et al.* Evidence of Vorticity and Shear at Large Angular Scales in the WMAP Data: A Violation of Cosmological Isotropy? // *Astrophys. J.* 2005. V. 629. P. L1; arXiv:astro-ph/0503213.
33. *Naselsky P. D. et al.* Understanding the WMAP Cold Spot Mystery // *Astrophys. Bull.* 2010. V. 65. P. 101.
34. *Haslam C. G. T. et al.* A 408 MHz All-Sky Continuum Survey. II. The Atlas of Contour Maps // *Astron. Astrophys.* 1982. V. 47. P. 1.
35. *Hansen M. et al.* Faraday Rotation as a Diagnostic of Galactic Foreground Contamination of Cosmic Microwave Background Maps // *MNRAS*. 2012. V. 426. P. 57; arXiv:1202.1711.
36. *Hansen F. K., Banday A. J., Górski K. M.* Testing the Cosmological Principle of Isotropy: Local Power-Spectrum Estimates of the WMAP Data // *MNRAS*. 2004. V. 354. P. 641.
37. *Park C.-G.* Non-Gaussian Signatures in the Temperature Fluctuation Observed by the Wilkinson Microwave Anisotropy Probe // *MNRAS*. 2004. V. 349. P. 313.
38. *Schwarz D. J. et al.* Is the Low- l Microwave Background Cosmic? // *Phys. Rev. Lett.* 2004. V. 93. P. 221301.
39. *Verkhodanov O. V., Khabibullina M. L., Majorova E. K.* Tessellated Mapping of Cosmic Background Radiation Correlations // *Astrophys. Bull.* 2009. V. 64. P. 263; arXiv:0912.3073.
40. *Verkhodanov O. V., Khabibullina M. L.* Dominant Multipoles in WMAP5 Mosaic Data Correlation Maps // *Astrophys. Bull.* 2010. V. 65. P. 390.
41. *Eriksen H. K. et al.* Testing for Non-Gaussianity in the Wilkinson Microwave Anisotropy Probe Data: Minkowski Functionals and the Length of the Skeleton // *Astrophys. J.* 2004. V. 612. P. 64.
42. *Eriksen H. K. et al.* The N-Point Correlation Functions of the First-Year Wilkinson Microwave Anisotropy Probe Sky Maps // *Astrophys. J.* 2005. V. 622. P. 58.
43. *Räth C., Schuecker P., Banday A. J.* A Scaling Index Analysis of the Wilkinson Microwave Anisotropy Probe Three-Year Data: Signatures of Non-Gaussianities and Asymmetries in the Cosmic Microwave Background // *MNRAS*. 2007. V. 380. P. 466.
44. *Verkhodanov O. V.* Radio and Optical Identification of Giant Radio Galaxies from NVSS Radio Survey // *Astrophys. Bull.* 2014. V. 69 (in press).
45. *Verkhodanov O. V.* Searching for Non-Gaussianity in the Observational Cosmic Microwave Background Data // *Phys. Usp.* 2012. V. 55. P. 1098.
46. *Ade P. A. R. et al. (BICEP2 Collab.)* BICEP2 I: Detection of B-Mode Polarization at Degree Angular Scales. arXiv:1403.3985.
47. *Liu H., Mertsch P., Sarkar S.* Fingerprints of Galactic Loop I on the Cosmic Microwave Background. arXiv:1404.1899.

48. *Ade P. A. R. et al. (Planck Collab.)*. Planck 2013 Results. XX. Cosmology from Sunyaev–Zeldovich Cluster Counts // *Astron. Astrophys.* 2014 (in press); arXiv:1303.5080.
49. *Ade P. A. R. et al. (Planck Collab.)*. Planck 2013 Results. XVI. Cosmological Parameters // *Astron. Astrophys.* 2014 (in press); arXiv:1303.5076.
50. *Spergel D., Flauger R., Hlozek R.* Planck Data Reconsidered. arXiv:1312.3313S.
51. *Doroshkevich A. G. et al.* The Gauss–Legendre Sky Pixelization for the CMB Polarization (GLESP-pol). Errors due to Pixelization of the CMB Sky // *Intern. J. Mod. Phys. D.* 2011. V. 20. P. 1053; arXiv:0904.2517.